

# Precision Timing Measurements of PSR J1012+5307

Ch. Lange,<sup>1</sup> F. Camilo,<sup>2</sup> N. Wex,<sup>1</sup> M. Kramer,<sup>3</sup> D.C. Backer,<sup>4</sup> A.G. Lyne,<sup>3</sup>  
O. Doroshenko<sup>1</sup>

<sup>1</sup>*Max Planck Institut für Radioastronomie, Auf dem Hügel 69, D-53121 Bonn, Germany*

<sup>2</sup>*Columbia Astrophysics Laboratory, Columbia University, 550 West 120th Street, New York, NY 10027, USA*

<sup>3</sup>*University of Manchester, Jodrell Bank Observatory, Macclesfield, Cheshire SK11 9DL, UK*

<sup>4</sup>*Astronomy Department, 601 Campbell Hall, University of California, Berkeley, California 94720-3411, USA*

21 January 2001

## ABSTRACT

We present results and applications of high precision timing measurements of the binary millisecond pulsar J1012+5307. Combining our radio timing measurements with results based on optical observations, we derive complete 3-D velocity information for this system. Correcting for Doppler effects, we derive the intrinsic spin parameters of this pulsar and a characteristic age of  $8.6 \pm 1.9$  Gyr. Our upper limit for the orbital eccentricity of only  $8 \times 10^{-7}$  (68% C.L.) is the smallest ever measured for a binary system. We demonstrate that this makes the pulsar an ideal laboratory to test certain aspects of alternative theories of gravitation. Our precision measurements suggest deviations from a simple pulsar spin-down timing model, which are consistent with timing noise and the extrapolation of the known behaviour of slowly rotating pulsars.

**Key words:** binaries: general — pulsars: general — pulsars: individual: J1012+5307 — gravitation — relativity — time

## 1 INTRODUCTION

The 5.3-ms pulsar J1012+5307 was discovered during a survey for short period pulsars with the 76-m Lovell radio telescope at Jodrell Bank. Nicastro et al. (1995) showed that the pulsar is in a binary system with an orbital period of 14.5 hr and a companion mass between  $0.11 M_{\odot}$  and  $0.25 M_{\odot}$  (90% confidence level, C.L.). Optical observations reported by Lorimer et al. (1995) revealed an optical counterpart within  $0''.2 \pm 0''.5$  of the pulsar timing position, consistent with its being a white dwarf (WD) companion of mass  $0.15 M_{\odot}$ .

Indeed, PSR J1012+5307 is one of the few examples of binary millisecond pulsars where optical observations of the WD companion considerably enhance our knowledge about the radio pulsar and its binary system (van Kerkwijk et al. 1996). Callanan et al. (1998), for instance, used their results from optical observations to obtain a number of essential pieces of information for this system. Comparing the measured optical luminosity to its value expected from WD models, they determined the distance to be  $d = 840 \pm 90$  pc. The Doppler shift of the measured H-spectrum of the WD companion gives an additional radial velocity component of  $44 \pm 8$  km s<sup>-1</sup> relative to the solar system barycentre, SSB. From the radial velocity (semi-)amplitude and the orbital parameters known from pulsar timing, the mass ratio between the pulsar and its companion is measured to be  $m_{\text{PSR}}/m_c = 10.5 \pm 0.5$ .

In order to derive the intrinsic spin-down age of mil-

lisecond pulsars, one needs to have accurate distance estimates to correct for apparent acceleration effects (Shklovskii 1970). A proper motion obtained by pulsar timing is usually converted into a transverse velocity by using a distance estimate derived from the dispersion in the interstellar medium, applying a model of the free electron density distribution (Taylor & Cordes 1993). However, this model yields a high level of systematic uncertainty (e.g. Toscano et al. 1999b). The dispersion measure (DM) distance of 520 pc is indeed somewhat smaller than the distance derived from luminosity models.

Applying classical cooling models (Iben & Tutukov 1986) for low mass WDs and the DM distance, Lorimer et al. derived an age of only 0.3 Gyr for the WD companion which was in apparent contradiction with the inferred spin-down age of the pulsar of 7 Gyr. However, Alberts et al. (1996) were able to model the binary parameters if they assumed that the cooling age of the WD is similar to the spin-down age of the pulsar. More recently, Driebe et al. (1998) modeled the cooling process of WDs, obtaining an age of  $6 \pm 1$  Gyr for the companion of PSR J1012+5307. Ergma et al. (1998) modeled evolutionary sequences of neutron stars with close low mass binary companions and short orbital periods, whilst Sarna et al. (1998) developed an evolutionary scenario for PSR J1012+5307, reproducing the observed binary period and companion mass. They modeled the age of the neutron star to be between 4.5 and 6.0 Gyr, whilst the

arXiv:astro-ph/0102309v1 18 Feb 2001

mass of the WD was found to be  $0.16 \pm 0.02 M_{\odot}$ , consistent with mass estimates derived by other models based on different observations and evolutionary models (Callanan et al. 1998; Driebe et al. 1998).

In this paper, we combine a set of high precision timing data with the information derived for the binary system from radio pulsar and optical WD observations as well as from model calculations. After a short description of the timing observations and data reduction techniques, we describe a new binary timing model that is important for the low eccentricity case, discuss the resulting solution using statistical tests, and present the derived timing parameters. These results are analysed in the following sections. We show that proper motion and Galactic acceleration of PSR J1012+5307 have a significant influence on the derived characteristic age. Furthermore, we obtain strong limits on the true eccentricity of the system and discuss its meaning for evolutionary scenarios. As a result of the stringent limits obtained both on the change in orbital period as well as on the true eccentricity of the system, we demonstrate that this binary system is highly suitable for testing different theories of gravitation.

## 2 OBSERVATIONS

### 2.1 Effelsberg timing

We have made regular high precision timing observations of PSR J1012+5307 since October 1996 using the 100-m radio telescope of the Max Planck Institut für Radioastronomie in Effelsberg near Bonn. The typical observing rate has been once per month with a usual observing time of about one hour. The overall post-fit RMS of the timing model applied to the 1213 resulting times-of-arrival (TOAs) is  $3.1 \mu\text{s}$ . Sometimes, however, the source shows strong intensity fluctuations on time scales of typically two hours caused by scintillation effects in the ionised component of the interstellar medium. We made use of these intensity maxima by optimising our observing strategy, i.e., staying “on source” until the pulsar becomes weaker again. As a consequence of this highly successful “scintillation hopping”, many TOAs are of much higher quality, with errors frequently smaller than  $1 \mu\text{s}$ . Figure 1 shows a typical example for the development of TOA uncertainties during a scintillation maximum. Since we have many such high quality TOAs covering several orbits, they proved to be extremely useful for the precise determination of orbital parameters.

#### 2.1.1 Receiving systems

Most of the data were obtained with a 1.3–1.7 GHz tunable HEMT receiver installed in the primary focus of the telescope. The noise temperature of this system is 25 K, resulting in a system temperature from 30 to 50 K on cold sky depending on elevation. The antenna gain at these frequencies is  $1.5 \text{ K Jy}^{-1}$ . An intermediate frequency (IF) centred on 150 MHz for left-hand (LHC) and right-hand (RHC) circularly polarised signals was obtained after down-conversion from a central RF frequency of usually 1410 MHz.

In order to monitor DM changes, occasionally we also obtained data at 860 and 2700 MHz. For the 860-MHz observations we used an uncooled HEMT-receiver operating in

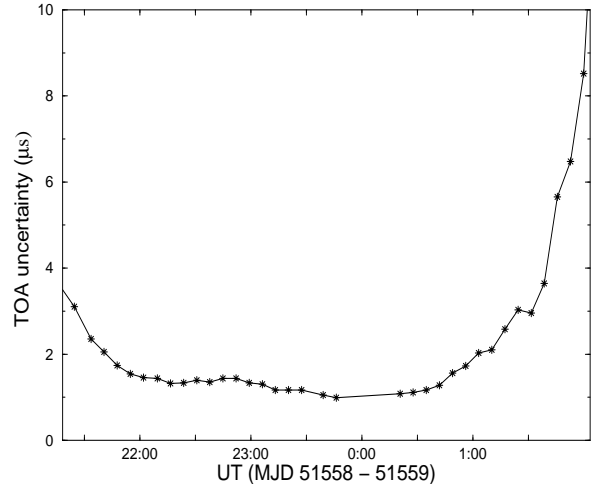


**Figure 1.** Errors of the TOAs during a scintillation maximum.

the primary focus with a bandwidth of 30 MHz. The system temperature during the observations was about 65 K on cold sky with a telescope gain of about  $1.5 \text{ K Jy}^{-1}$ . The 2700-MHz data were obtained with a cooled HEMT receiver in the secondary focus, with a system temperature of typically 50 K on cold sky. As for the other receivers, LHC and RHC signals were mixed down to an IF of 150 MHz.

#### 2.1.2 Coherent De-Disperser

The signals received from the telescope were acquired and processed with the Effelsberg-Berkeley Pulsar Processor (EBPP) which removes the dispersive effects of the interstellar medium on-line using the technique of “coherent de-dispersion” (Hankins & Rickett 1975). Before entering the EBPP, the two IF LHC and RHC signals are converted to an internal IF of 440 MHz. A maximum bandpass of  $112 \text{ MHz}^*$  is split into four independent portions for both circular polarisations. Each portion is mixed down to baseband and subdivided into 8 narrow channels via a set of digital filters (Backer et al. 1997) for coherent online de-dispersion by convolution using a custom VLSI device. In total 64 output signals are detected and integrated in phase with the predicted topocentric pulse period.

#### 2.1.3 Arrival times measurements

A TOA was calculated for each average profile obtained during a 5–10 min observation. During this process, the observed time-stamped profile was compared to a synthetic template, which was constructed out of 12 Gaussian components fitted to a high signal-to-noise standard profile (see Kramer et al. 1998; 1999). This template matching was done by a least-squares fitting of the Fourier-transformed data (Taylor 1991). The final TOA was obtained by using the

\* The bandwidth available depends on observing frequency and DM of the pulsar. At 1.41 GHz we used a bandwidth of 56 MHz for PSR J1012+5307.

measured time delay between the actual profile and the template, and the accurate time stamp of the data provided by a local H-maser and corrected off-line to UTC(NIST) using recorded information from the satellites of the Global Positioning System (GPS). The uncertainty of each TOA was estimated using a method described by Downs & Reichley (1983).

## 2.2 Jodrell Bank timing

Since its discovery in 1993, PSR J1012+5307 has been regularly monitored using the 76-m Lovell telescope at Jodrell Bank with cryogenic receivers at 408, 606, and 1404 MHz. Both LHC and RHC signals were observed using a  $2 \times 64 \times 0.125$ -MHz filter bank at 408 and 606 MHz and a  $2 \times 32 \times 1.0$ -MHz filter bank at 1404 MHz. After detection, the signals from the two polarisations were filtered, digitised at appropriate sampling intervals, and incoherently de-dispersed in hardware before being folded on-line with the topocentric pulse period and written to disk. Each integration was typically of 1–3 minutes duration; 6 or 12 such integrations usually constituted an observation. In the analysis stage, the profiles were added in polarisation pairs before being summed to produce a single total-intensity profile. A standard pulse template was fitted to the observed profiles at each frequency to determine a total of 400 pulse TOAs. Details of the observing system and the data reduction scheme can be found elsewhere (e.g. Bell et al. 1997).

Although the templates used in the Effelsberg and Jodrell Bank data reduction differed, resulting offsets were absorbed in a global least-squares fit. The typical measurement accuracy of the Jodrell Bank 1404 MHz timing data is about 9  $\mu$ s.

## 3 PRECISION TIMING

The combined TOAs, corrected to UTC(NIST) and weighted by their individual uncertainties determined in the fitting process, were analysed with the TEMPO software package<sup>†</sup>, using the DE200 ephemeris of the Jet Propulsion Laboratory (Standish 1990). Owing to the extremely low eccentricity of this system, we applied a binary timing model that uses the Laplace Lagrange parameters  $\eta$  and  $\kappa$  and the time of ascending node  $T_{\text{ASC}}$  in place of the Keplerian parameters  $e$ ,  $\omega$  and  $T_0$  (see Appendix A for details). The Keplerian parameters as a function of those used by the model can be calculated as

$$e = \sqrt{\kappa^2 + \eta^2} \quad (1)$$

$$\omega = \arctan(\eta/\kappa) \quad (2)$$

$$T_0 = T_{\text{ASC}} + \frac{P_b}{2\pi} \arctan(\eta/\kappa). \quad (3)$$

TEMPO minimizes the sum of weighted squared timing residuals, i.e., the difference between observed and model TOAs,  $r_i$ , yielding a set of improved pulsar parameters and post-fit timing residuals. The timing residuals shown in Fig. 2 indicate deviations from the timing model which are slightly larger than the calculated TOA uncertainties,

$\sigma_i$ . This most likely stems from a small underestimation of the error in the TOAs. The data uncertainties used in the following were scaled by an appropriate factor to achieve a uniform reduced  $\chi^2 = 1$  for each data set. In order to test the statistical properties of our data we have generated histograms of the deviations of the timing residuals from the model. The final residuals show the expected Gaussian distribution (Fig. 3).

In order to search for systematic errors that are either small enough to be individually undetectable or have a time dependence which approximates some linear combination of terms in the model, we have searched for tell-tale correlations among nearly adjacent post-fit residuals (cf. Taylor & Weisberg 1989). We combined 2, 4, 8 etc. consecutive TOAs and evaluated the average residual of the remaining data set. A “clean” data set should exhibit a slope of  $-0.5$  in a plot of RMS versus number of combined TOAs. The results, as shown in Fig. 4, show no or very little correlation among Effelsberg data and the Jodrell Bank data recorded at 410 MHz after employing the timing model described in Table 1. The Jodrell Bank data at 1400 MHz and 606 MHz exhibit, however, some correlation. We tested for possible impact of these correlations on the fit parameters by analysing the timing data without one or both of these data sub-sets. The parameters derived from these reduced data sets did not significantly differ from those derived by the fit to all the data.

The final parameters obtained from fitting the timing model to our data of PSR J1012+5307 are shown in Table 1. The upper limits on the derivatives of  $e$ ,  $x$  and  $P_b$  were obtained by separately fitting for each of them. These were set to zero during the fits for all other parameters. The residuals show slow variations that can be removed by fitting for  $\ddot{P}$ . We do not believe that instrumental effects can account for this effect but rather suggest that the measurement reflects rotational instabilities in the pulsar. In this case, PSR J1012+5307 is only the second Galactic field millisecond pulsar to show a significant second spin frequency derivative,  $\ddot{\nu}$ , the other being PSR B1937+21 (Kaspi et al. 1994)<sup>‡</sup>. We will discuss the possible important implications of this result in Section 6.

## 4 INTRINSIC PULSAR PARAMETERS

As summarised in Section 1 the binary millisecond pulsar PSR J1012+5307 is unique since the combination of optical and radio measurements allows a full determination of the motion of the system through space and also the determination of several intrinsic parameters.

### 4.1 3-D velocity

The full 3-d motion of the pulsar relative to the SSB is determined by combining the timing proper motion with distance to the system obtained from luminosity models for

<sup>‡</sup> Cognard et al. (1996) measured a  $\ddot{\nu}$  for the millisecond pulsar B1821–24 located in a globular cluster. Here the acceleration by the cluster gravitational potential may significantly affect the observed spin-down parameters.

<sup>†</sup> <http://pulsar.princeton.edu/tempo>

Right Ascension, $\alpha$ (J2000)	$10^{\text{h}}12^{\text{m}}33^{\text{s}}.43370(3)$
Declination, $\delta$ (J2000)	$53^{\circ}07'02''.5884(4)$
$\mu_{\alpha}$ (mas yr $^{-1}$ )	$2.4(2)$
$\mu_{\delta}$ (mas yr $^{-1}$ )	$-25.2(2)$
$\nu$ (Hz)	$190.267837621903(4)$
$\dot{\nu}$ (s $^{-2}$ )	$-6.2029(4) \cdot 10^{-16}$
$\ddot{\nu}$ (s $^{-3}$ )	$-9.8(2.1) \cdot 10^{-27}$
$P$ (ms)	$5.2557490141197(1)$
$\dot{P}$	$1.7134(1) \cdot 10^{-20}$
$\ddot{P}$ (s $^{-1}$ )	$5.1(1.1) \cdot 10^{-31}$
Epoch (MJD)	50700.0
Dispersion Measure (DM) (cm $^{-3}$ pc)	9.0233(2)
Orbital period, $P_b$ (days)	0.60467271355(8)
Proj. semi-major axis, $x$ (s)	0.5818172(2)
$\eta$	$0.9(8) \cdot 10^{-6}$
$\kappa$	$0.01(80) \cdot 10^{-6}$
$T_{\text{ASC}}$ (MJD)	50700.0816290(1)
Upper limits:	
Parallax, $\pi$ (mas)	$< 1.3$
$e$	$< 1.3 \cdot 10^{-6} \text{ }^a$
$\dot{e}$ (s $^{-1}$ )	$< 2 \cdot 10^{-14}$
$\dot{x}$	$< 1.4 \cdot 10^{-14}$
$\dot{P}_b$	$< 1 \cdot 10^{-13}$
DM (cm $^{-3}$ pc yr $^{-1}$ )	$< 1.2 \cdot 10^{-4}$

<sup>a</sup> See section 4.4 for details.

**Table 1.** Timing parameters for the millisecond pulsar J1012+5307. Quoted errors correspond to twice the errors derived by TEMPO. Upper limits represent 95% C.L.

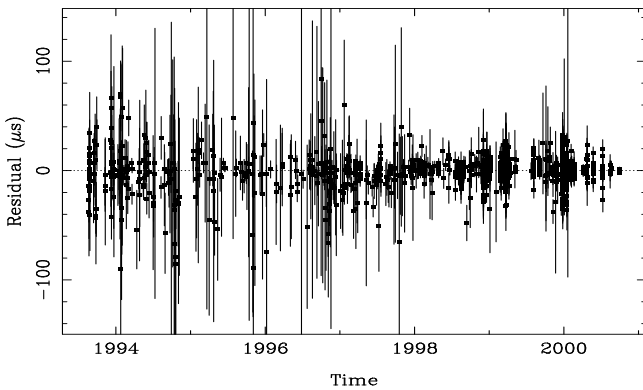


**Figure 2.** Post-fit timing residuals as a function of observing year.

the white dwarf companion,  $d = 840 \pm 90$  pc. This distance is consistent with the obtained upper limit for the timing parallax. Given the pulsar's ecliptic latitude of  $38^\circ$ , it is not unexpected that a significant value for the timing parallax could not be obtained. We derive transverse velocities of

$$v_{\alpha} = \mu_{\alpha} \cdot d = 8.8 \pm 1.2 \text{ km s}^{-1} \quad (4)$$

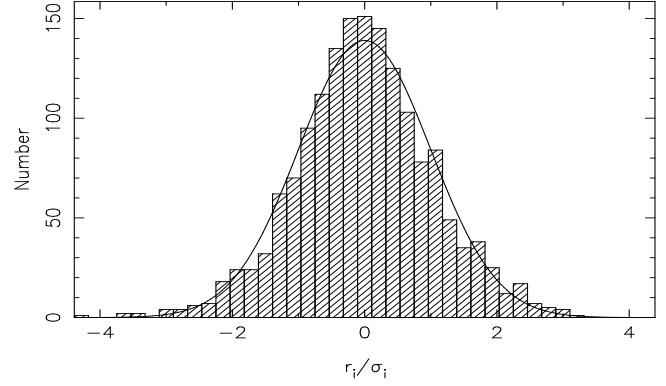


**Figure 3.** Distribution of all post-fit timing residuals normalized by their uncertainties.

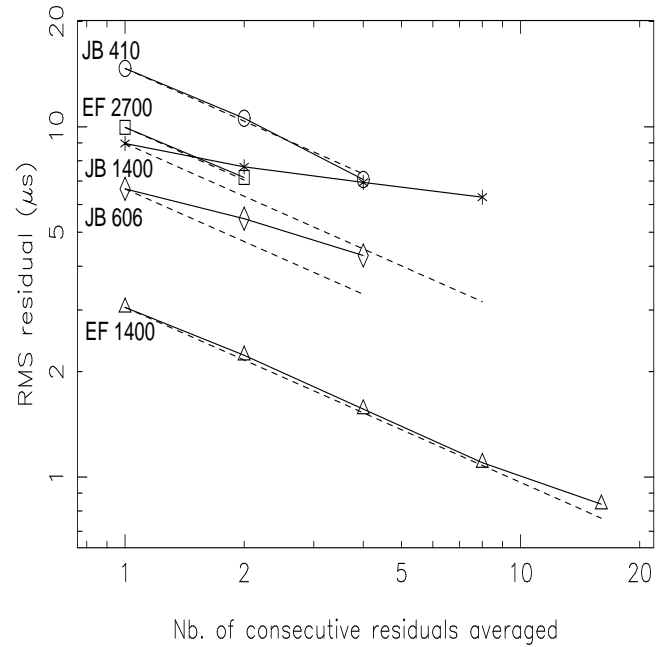


**Figure 4.** Mean post-fit RMS residuals of the data sets versus the number of consecutive averaged timing residuals. The symbols represent data from: EBPP 1.4 GHz ( $\Delta$ ) and 2.7 GHz ( $\square$ ), and Jodrell Bank 410 MHz ( $\circ$ ), 606 MHz ( $\diamond$ ), and 1.4 GHz ( $*$ ). The 870 MHz data from Effelsberg are not included here owing to their small number.

$$v_{\delta} = \mu_{\delta} \cdot d = -102 \pm 11 \text{ km s}^{-1}. \quad (5)$$

Optical measurements (cf. Section 1) yield a radial velocity component of  $+44(8) \text{ km s}^{-1}$ . Hence, the total velocity of the system is  $111(28) \text{ km s}^{-1}$ . This value is consistent with the average space velocity of millisecond pulsars of  $130 \text{ km s}^{-1}$  estimated by Lyne et al. (1998) and Toscano et al. (1999a).

## 4.2 Doppler effects

Due to the motion of PSR J1012+5307 relative to the solar system, any period  $P^{\text{obs}}$  of the pulsar spin or binary system, measured at the SSB, differs from the period  $P^{\text{int}}$  in the pulsar reference frame by a Doppler factor  $D$ . Follow-

ing Damour & Taylor (1991), we write the relation between these periods

$$P^{\text{obs}} = D P^{\text{intr}} \equiv \left(1 + \frac{\mathbf{n} \cdot \mathbf{v}_r}{c}\right) P^{\text{intr}} + \mathcal{O}(v_r^2/c^2) \quad (6)$$

with  $\mathbf{n}$  the unit vector to the pulsar and  $\mathbf{v}_r$  the relative velocity between the pulsar and the SSB (Damour & Taylor 1992). As  $v_r/c$  is typically less than 0.1% for millisecond pulsars, this Doppler shift is for most purposes unimportant. Hence, we will for the rest of this paper denote  $P^{\text{obs}}$  as  $P$ . However, the period derivative may be modified by the relative motion.

Calculating the time-derivative of Eqn. 6 and separating the effect of the proper motion of the system (Shklovskii 1970) from the influence of the Galactic acceleration, we derive as contributions to the period derivative

$$\dot{P}^{\text{obs}} = \dot{P}^{\text{intr}} D + \dot{P}^{\text{Shk}} + \dot{P}^{\text{Gal}}, \quad (7)$$

where the difference of the constant Doppler factor  $D$  from unity may be neglected. The contributions  $\dot{P}^{\text{Shk}} + \dot{P}^{\text{Gal}} \equiv \dot{P}^D$  are written explicitly

$$\dot{P}^{\text{Shk}} = \frac{1}{c} \mu^2 d P \quad (8)$$

$$\dot{P}^{\text{Gal}} = \frac{1}{c} (\mathbf{n}_{\text{psr}} \cdot [\mathbf{a}_{\text{psr}} - \mathbf{a}_e]) P, \quad (9)$$

where  $d$  is the distance to the pulsar. Here  $\mathbf{n}_{\text{psr}}$  is the position vector to the pulsar,  $\mu$  its proper motion and  $\mathbf{a}_{\text{psr}}$  and  $\mathbf{a}_e$  the Galactic acceleration of the pulsar and the Earth, respectively. We measure  $\mathbf{n}_{\text{psr}}$  and  $\mu$  from our timing observations. The small correction term  $\dot{P}^{\text{Gal}}/P = -7 \times 10^{-20} \text{s}^{-1}$  for the Galactic acceleration is obtained applying a model for the Galactic potential (Carlberg & Innanen 1987; Kuijken & Gilmore 1989). Inserting these parameters into Eqns. 8 and 9, we obtain a Doppler correction of

$$\dot{P}^D/P = 1.4 \pm 0.3 \times 10^{-18} \text{s}^{-1}. \quad (10)$$

Its error is dominated by the uncertainty in the distance to the pulsar.

### 4.3 Characteristic age

We can now use our timing results to obtain the true spin-down age, the so-called characteristic age of PSR J1012+5307. With a spin period of  $P = 5.256 \text{ ms}$  and a Doppler factor as given in Eqn. 10, we derive a Doppler correction of

$$\dot{P}^D = 7.4 \pm 1.6 \times 10^{-21}, \quad (11)$$

which has to be subtracted from the measured  $\dot{P}$  before calculating the intrinsic characteristic age of the system:

$$t_{\text{char}}^{\text{intr}} = \frac{P}{2\dot{P}^{\text{intr}}} = \frac{P}{2(\dot{P}^{\text{obs}} - \dot{P}^D)} = 8.6 \pm 1.9 \text{ Gyr}. \quad (12)$$

We note that the characteristic age assumes magnetic dipole braking (i.e., braking index of 3) and is only a realistic estimate of the real pulsar age if the initial spin period was sufficiently small (Camilo et al. 1994). Although this may not apply to He-WD binaries (Backer 1998), the characteristic age is in reasonable agreement with a cooling age of the white dwarf as derived by evolutionary models (Alberts et al. 1996; Sarna et al. 1998; Driebe et al. 1998).

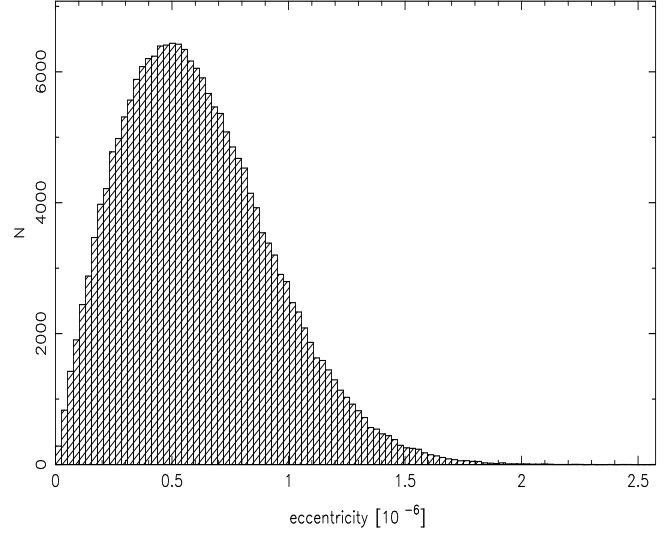


**Figure 5.** Distribution of values for the real eccentricity from simulated parameters (see text).

### 4.4 Orbital eccentricity

In Appendix A we analyse the contribution of the Shapiro delay for binary orbits with moderate inclination angles and negligible intrinsic eccentricities to the apparent eccentricity of the system. As we show, the Shapiro delay cannot be separated from the Roemer delay, which leads to a small correction to the observed eccentricity. In order to investigate this effect for PSR J1012+5307 quantitatively and to obtain the true orbital eccentricity, we make use of independent determinations of the system parameters.

From the companion mass of  $0.16(2) M_{\odot}$ , the measured mass ratio of  $q \equiv m_p/m_c = 10.5(5)$ , and the mass function

$$f_m \equiv \frac{m_c^3 \sin^3 i}{(m_c + m_p)^2} = 0.000578 M_{\odot} \quad (13)$$

obtained from the timing analysis, we derive the range  $r$  and shape  $s$  of the Shapiro delay in the system according to

$$r[\mu\text{s}] = 4.9255 (m_c/M_{\odot}) \quad \text{and} \quad (14)$$

$$s \equiv \sin i = \left( \frac{f_m (q+1)^2}{m_c} \right)^{1/3}. \quad (15)$$

The resulting shape parameter of  $s \approx 0.8$  indicates a moderate inclination of the system, i.e.,  $i = 52^\circ$  or  $128^\circ$ . The contribution of the Shapiro delay to the observed  $\eta$  is calculated according to Eqn. A22 and subtracted from the measured value. Applying Eqn. 1, we obtain upper limits on the true eccentricity of

$$\begin{aligned} e^{\text{intr}} &< 0.8 \times 10^{-6} \quad (68\% \text{ C.L.}) \\ e^{\text{intr}} &< 1.3 \times 10^{-6} \quad (95\% \text{ C.L.}), \end{aligned} \quad (16)$$

which were derived from Monte Carlo simulations. In these calculations, whose results are displayed in Fig. 5, we simulated the parameters  $q$  and  $m_c$  and the observed  $\kappa$  and  $\eta$  in accordance with the observational uncertainties.

## 5 TESTS OF THEORIES OF GRAVITATION

### 5.1 Dipole gravitational waves

Unlike general relativity, many alternative theories of gravity predict the presence of a radiative monopole and dipole as well as the quadrupole and higher order multipoles (Will 1993). Scalar-tensor theories, for instance, predict for binary systems a loss of orbital energy which is at highest order dominated by scalar dipole radiation. As a result, the period  $P_b$  of a circular orbit will change with

$$\dot{P}_b^{\text{dipole}} \simeq -\frac{4\pi^2 G_*}{c^3 P_b} \frac{m_p m_c}{m_p + m_c} (\alpha_p - \alpha_c)^2, \quad (17)$$

where  $G_*$  is the bare gravitational constant,  $c$  is the speed of light and  $m_p$  and  $m_c$  the mass of the pulsar and its companion (Damour & Esposito-Farèse 1996). The parameters  $\alpha_p$  and  $\alpha_c$  represent the effective coupling strengths of the scalar field to the pulsar and its companion, respectively.

Damour & Esposito-Farèse (1996) show that  $\alpha_c$  can be neglected compared to  $\alpha_p$ , since the gravitational binding energy per unit mass of a WD,  $\varepsilon_{\text{WD}} \equiv E^{\text{grav}}/mc^2 \approx 10^{-4}$ , is very much smaller than that of a 1.4- $M_\odot$  neutron star,  $\varepsilon_p \approx 0.15$ .

Using this assumption, and taking  $G_* \approx G$ , Eqn. 17 can be approximated as:

$$\dot{P}_b^{\text{dipole}} \simeq -\frac{4\pi^2 G}{c^3 P_b} m_c \frac{q}{q+1} \alpha_p^2. \quad (18)$$

Since all terms except  $\alpha_p$  in this equation are measured, the effective coupling strength of PSR J1012+5307 can be restricted by limits on  $\dot{P}_b$ . We will show that these are the tightest bounds on  $\alpha_p^2$  ever measured for a neutron star.

The observable rate of change of the orbital period of PSR J1012+5307 is the sum of several contributions, either intrinsic to the orbit or caused by projection effects:

$$\dot{P}_b = \dot{P}_b^{\text{D}} + \dot{P}_b^{\text{GR}} + \dot{P}_b^{\dot{G}} + \dot{P}_b^{\text{dipole}} \quad (19)$$

(Damour & Taylor 1991). Here, the Doppler correction of  $\dot{P}_b$  is given by  $\dot{P}_b^{\text{D}}$  and the contribution  $\dot{P}_b^{\text{GR}}$  represents gravitational radiation as predicted by general relativity. The values of these effects can be estimated and may be subtracted from the measured value of  $\dot{P}_b$ . The additional contributions  $\dot{P}_b^{\dot{G}}$  and  $\dot{P}_b^{\text{dipole}}$  represent the period derivative due to a change of the gravitation constant and due to gravitational dipole radiation, respectively. All terms of gravitational radiation not accounted for are of the order  $c^{-5}$  or higher. We derive  $\dot{P}_b^{\text{D}}$  from Eqn. 10, with the orbital period of 52 240 s, to be

$$\dot{P}_b^{\text{D}} = 7.3 \pm 1.6 \times 10^{-14}. \quad (20)$$

The orbital period decay derived from the theory of general relativity for a circular orbit can be approximated to

$$\dot{P}_b^{\text{GR}} \simeq -\frac{384\pi^2}{5} \frac{(G m_c)^{5/3}}{P_b^{5/3} c^5} \frac{q}{(q+1)^{1/3}} \approx -1.0 \pm 0.2 \times 10^{-14}, \quad (21)$$

using the WD-mass  $m_c = 0.16(2) M_\odot$  and the mass ratio of  $q \approx 10.5$  between the pulsar and the WD (Callanan et al. 1998).

A variation in the orbital period as a result of a possible time dependence of the gravitational constant can for this system be approximated to

$$\dot{P}_b^{\dot{G}} \approx -2 \frac{\dot{G}}{G} (1 + c_p) P_b \quad (22)$$

(Nordtvedt 1990) where  $c_p$  is the compactness of the pulsar, which is approximately two times its binding energy. Using the upper limit  $|\dot{G}/G| \lesssim 8 \times 10^{-12} \text{yr}^{-1}$  (Williams et al. 1996) we can restrict

$$|\dot{P}_b^{\dot{G}}| \lesssim 3.6 \times 10^{-14}. \quad (23)$$

This value is only about 1/3 of our 1- $\sigma$  error for  $\dot{P}_b$ . We can therefore exclude a significant influence on  $\dot{P}_b$  from this effect.

Subtracting the known contributions from the limit measured for  $\dot{P}_b$  yields a value of  $\dot{P}_b^{\text{dipole}} \approx -0.6(1.1) 10^{-13}$ . Using this value we obtain limits for  $\alpha_p$  of

$$\begin{aligned} \alpha_p^2 &< 2 \times 10^{-4} && (68\% \text{ C.L.}) \\ \alpha_p^2 &< 4 \times 10^{-4} && (95\% \text{ C.L.}), \end{aligned} \quad (24)$$

where we have taken into account uncertainties in the parameter values used.

Simulations of future observations show that the precision of the measurement of  $\dot{P}_b$  will increase significantly. A continuation of our timing observations with an accuracy and observing rate similar to that of the past few years will lead to an improvement by a factor of about 3 within the next three years. The applicability of this improvement for the value of  $\alpha_p$  might be reduced by the unknown contribution of  $\dot{G}$ , unless the limits on this parameter are also improved. It is also desirable that the distance to PSR J1012+5307 be determined with higher accuracy to allow a more reliable estimate of the transverse Doppler effect.

### 5.2 Local Lorentz invariance

Will & Nordtvedt (1972) pointed out that one expects the existence of a preferred cosmic rest frame for gravitational interaction if gravity is mediated in part by a long range vector field or by a second tensor field. In the post-Newtonian limit all the gravitational effects associated with such a preferred frame are phenomenologically describable by two parameters,  $\alpha_1$  and  $\alpha_2$ . Only in gravity theories without a preferred frame, e.g. general relativity, are the values of these parameters equal to zero.

A consequence of a preferred cosmic rest frame would be the introduction of an eccentricity into orbits of gravitationally bound bodies of different masses which are in motion relative to this preferred frame. This effect is quantified by the parameter  $\alpha_1$ . Wex (2000) has applied a statistical analysis of all pulsar binary systems to find limits for this parameter. This analysis yields  $|\alpha_1| < 1.4 \times 10^{-4}$  at 95% C.L. Due to its extremely low true eccentricity and the known three dimensional proper motion, the data presented here for PSR J1012+5307 and included in Wex's analysis play a central role in this analysis. They might provide more stringent tests of local Lorentz invariance, if the real eccentricity of the system is even smaller and better observational limits on it are found.

## 6 DISCUSSION

### 6.1 Timing noise

Over the observed time span of about 7 years, PSR J1012+5307 shows a significant deviation from a sim-

ple  $\nu$ - $\dot{\nu}$  spin down behaviour. In order to model this effect, the spin-down model can be extended by allowing for a non-zero second derivative of the spin frequency,  $\ddot{\nu}$  (e.g. Cordes & Downes 1985). However, rather than being the result of rotational irregularities of the neutron star itself, a possible alternative explanation for a second spin frequency derivative could be a third order term of the proper motion,

$$\ddot{\nu}^D = -3 \frac{v_r}{c} \mu^2 \nu_{\text{intr}} - 2 \frac{d\mu^2}{c} \dot{\nu}_{\text{intr}}, \quad (25)$$

where  $v_r$  is the radial velocity of the system (Phinney 1992). This term can be computed and it is of order  $10^{-30} \text{ s}^{-3}$ , i.e., too small to explain the measured effect.

In order to investigate the possibility that the observed timing noise is caused by small changes in the DM, we modeled our multi-frequency data with a simultaneous fit of  $\ddot{\nu}$  and a second-order polynomial for DM. While  $\dot{\text{DM}}$  and  $\ddot{\text{DM}}$  were not significant, the  $\ddot{\nu}$  measurement was still a  $5\text{-}\sigma$  effect. The upper limit on  $\dot{\text{DM}}$  given in Table 1 is interestingly much smaller than one would expect for  $\text{DM}=9.02 \text{ cm}^{-3} \text{ pc}$  (Backer et al. 1993).

As a possible explanation, a second period derivative in the timing residuals can also be the result of a second light companion in a wider orbit (Thorsett et al. 1999). Assuming a circular orbit and an intermediate orbital phase, the measured value for  $\ddot{\nu}$  can be explained with e.g. a planet of terrestrial mass at  $\sim 30 \text{ AU}$  distance or a Jupiter-like planet at  $\sim 170 \text{ AU}$  distance from the centre of mass. Future observations will show if the timing residuals can be explained by a second Keplerian orbit.

However, it is more likely that the irregularities are intrinsic to the pulsar itself. Timing noise has been studied for normal, slowly rotating pulsars. Arzoumanian et al. (1994), for instance, defined the stability parameter

$$\Delta(t) \equiv \log \left( \frac{|\ddot{\nu}|}{6\nu} t^3 \right), \quad (26)$$

where  $t$  is the observing span which in their case was  $10^8 \text{ s}$ . Despite noticeable scatter, they obtained a correlation of this parameter with the period derivative for slowly rotating pulsars. This correlation predicts a value of  $\Delta_8 \approx -5.3$  for PSR J1012+5307. Using timing data over a time span  $10^8 \text{ s}$ , we measure a value of  $\Delta_8 \approx -5$ . Given that the fit leading to Arzoumanian et al.'s relation was made by eye, both values are in excellent agreement, in particular given the large scatter seen for normal pulsars. Moreover, the value of the second spin frequency derivative,  $\ddot{\nu} = -9.8(2.1) \times 10^{-27} \text{ s}^{-3}$ , is similar to the value of  $\ddot{\nu}$  published for PSR B1937+21 (Kaspi et al. 1994). Both sources exhibit a  $\Delta_8$  consistent with the correlation derived by Arzoumanian et al. Although we cannot yet completely rule out a different origin of the measured period second derivative, the value determined is apparently consistent with what is known for timing noise from normal pulsars. Assuming that we are now indeed observing rotational irregularities in two Galactic field millisecond pulsars, being consistent with the behaviour of normal pulsars extrapolated to very small period derivatives, it may indicate that the empirical relation found by Arzoumanian et al. is generally valid for millisecond pulsars as well as for normal pulsars. As other millisecond pulsars are now being monitored with similar timing precision over similar time spans, this conjecture can be tested. It may well be the case that

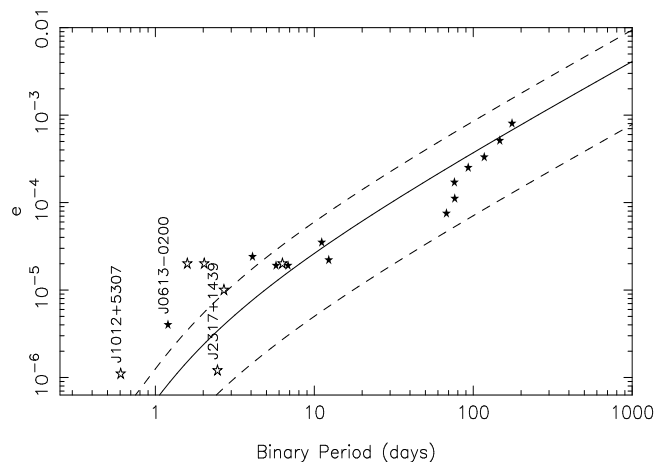


**Figure 6.** Relation between binary period and orbital eccentricity (filled symbols are measurements, open symbols upper limits) in binary systems with a millisecond pulsar and white dwarf companion.

we are finally exploring the ultimate accuracy of the pulsar clockwork, deciding over the suitability of millisecond pulsars as potential standards of time.

## 6.2 Orbital eccentricity — a relic of binary evolution

The convective fluctuation-dissipation theory of Phinney (1992) predicts a strong correlation between the orbital eccentricities and orbital periods of binary pulsars that have been recycled by stable mass-transfer from a Roche-lobe-filling, low-mass red giant. The measurements and upper limits for the orbital eccentricities of systems with appropriate evolutionary history are plotted in Fig. 6. They are, with the exception of PSR J0613–0200, in excellent agreement with the model of Phinney & Kulkarni (1994; curves in Fig. 6).

The lowest orbital eccentricity of a millisecond binary pulsar system known is the upper limit of  $1.3 \times 10^{-6}$  (68% C.L.) derived by Camilo et al. (1996) for PSR J2317+1439, which has an orbital period of 2.5 days. While this source follows the predicted trend, the eccentricity of the 1.2-d binary pulsar J0613–0200 has been determined to be  $3.8 \pm 1.0 \times 10^{-6}$ , which exceeds the 95% C.L. of this model relation by a factor of about 2.5 (Fig. 6). However, Phinney & Kulkarni (1994) pointed out that for extremely close binary systems the orbital eccentricity is difficult to model. Therefore, it is interesting to note that the upper limit for the eccentricity of the 0.6-d binary pulsar J1012+5307 of only  $e < 0.8 \times 10^{-6}$  (68% C.L.) is significantly lower than that of PSR J0613–0200.

## 6.3 Future observations

The motion of the binary system relative to the SSB results in a change of the orbital inclination that causes a variation in the projected semi-major axis of the system (Arzoumanian et al. 1996; Kopeikin 1996; Bell et al. 1997; Sandhu et al. 1997). The amplitude of this effect is given by

$$\dot{x}_\mu = 1.54 \times 10^{-16} x \cot i (-\mu_\alpha \sin \Omega + \mu_\delta \cos \Omega) \quad (27)$$

where  $\Omega$  is the position angle of the ascending node and  $\mu_\alpha$  and  $\mu_\delta$  the components of the proper motion in  $\text{mas yr}^{-1}$ . Given the value of the orbital inclination  $\sin i \approx 0.8$  as determined from the white dwarf optical light curve, a measurement of  $\dot{x}$  allows one to restrict the orbital orientation  $\Omega$ . Using our current data set, we derive a  $1\text{-}\sigma$  uncertainty for  $\dot{x}$  that is about twice the value expected for a perfect alignment between  $\Omega$  and  $\mu$ . Continuing timing observation will permit the measurement of this effect. Simulations, assuming an accuracy and data-taking rate similar to those at present, show that a  $3\text{-}\sigma$  detection of  $\dot{x}$  should be possible within the next four or five years. This would finally complete our knowledge of the full orientation and motion of the PSR J1012+5307 system.

## 7 SUMMARY

We have performed long-term high-precision timing observations of PSR J1012+5307. Combining our measurements with results based on optical observations, we derived complete 3-D velocity information for this system, permitting the correction of the measured spin parameters for Doppler effects. Due to the precision of our measurements and the extremely small eccentricity of this binary pulsar, we could use it as an ideal laboratory to test certain aspects of theories of gravitation. The deviation of the timing data from a simple spin-down model is probably due to rotational instabilities which are consistent with the extrapolation of the known spin-down behaviour of slowly rotating pulsars, suggesting that this phenomenon is a common property of most pulsars.

## ACKNOWLEDGEMENTS

We are grateful to all staff at the Effelsberg and Jodrell Bank observatories for their help with the observations. F.C. is supported by NASA grant NAG 5-9095. O.D. acknowledges the receipt of an Alexander-von-Humboldt fellowship.

## REFERENCES

- Alberts F., Savonije G.J., van den Heuvel E.P.J., Pols O.R., 1996, *Nature*, 380, 676
- Arzoumanian Z., Joshi K., Rasio F., Thorsett S.E., 1996, in *Pulsars: Problems and Progress*, IAU Colloquium 160, eds. S. Johnston, M. A. Walker, M. Bailes, ASP, San Francisco, p. 525
- Arzoumanian Z., Nice D.J., Taylor J.H., Thorsett S.E., 1994, *ApJ*, 422, 671
- Backer D.C., 1998, *ApJ*, 493, 873
- Backer D.C., Hama S., Van Hook S., Foster R.S., 1993, *ApJ*, 404, 636
- Backer D.C., Dexter M.R., Zepka A., Ng D., Werthimer D.J., Ray P.S., Foster R.S., 1997, *PASP*, 109, 61
- Bell J.F., Bailes M., Manchester R.N., Lyne A.G., Camilo F., Sandhu J.S., 1997, *MNRAS*, 286, 463
- Blandford R.D. & Teukolsky S.A., 1976, *ApJ*, 205, 580
- Callanan P.J., Garnavich P.M., Koester D., 1998, *MNRAS*, 298, 207
- Camilo F., Thorsett S.E., Kulkarni S.R., 1994, *ApJ*, 421, L15
- Camilo F., Nice D.J. & Taylor J.H., 1996, *ApJ*, 461, 812
- Carlberg R.G. & Innanen K.A., 1987, *AJ*, 94, 666
- Cordes J.M. & Downs G.S., 1984, *ApJSS*, 59, 343
- Cognard I., Bourgois G., Lestrade J.-F., Biraud F., Aubry D., Darchy B., Drouhin J.-P., 1996, *A&A*, 311, 179
- Damour T. & Taylor, 1991, *ApJ*, 366, 501
- Damour T. & Taylor, 1992, *Phys. Rev. D*, 45, 1840
- Damour T. & Esposito-Farèse G., 1996, *Phys. Rev. D*, 54, 1474
- Downs G.S., Reichley P.E., 1983, *ApJSS*, 53, 169
- Driebe T., Schönberner D., Blöcker T., Herwig F., 1998, *A&A*, 339, 123
- Ergma E., Sarna M.J., Antipova J., 1998, *MNRAS*, 300, 352
- Hankins T.H., Rickett B.J., 1975, in *Methods in Computational Physics 14*, eds. B. Alder, S. Fernbach, W. Rotenberg, Academic Press, New York, p. 55 - 129
- Iben I., Tutukov A.V., 1986, *ApJ*, 311, 742
- Kaspi V.M., Taylor J.H., Ryba M.F., 1994, *ApJ*, 428, 713
- Kopeikin S.M., 1996, *ApJ*, 467, L93
- Kramer M., Xilouris K. M., Lorimer D. R., Doroshenko O., Jessner A., Wielebinski R., Wolszczan A., Camilo F., 1998, *ApJ*, 501, 270
- Kramer M., Lange C., Lorimer D. R., Backer D. C., Xilouris K. M., Jessner A., Wielebinski R., 1999, *ApJ*, 526, 324
- Kuijken K. & Gilmore G., 1989, *MNRAS*, 239, 571
- Lorimer D.R., Lyne A.G., Festin L., Nicastro L., 1995, *Nature*, 376, 393
- Lyne A.G., Manchester R.N., Lorimer D.R., Bailes M., D'Amico N., Tauris T.M., Johnston S., Bell J.F., Nicastro L., 1998, *MNRAS*, 295, 743
- Nicastro L., Lyne A.G., Lorimer D.R., Harrison P.A., Bailes M., 1995, *MNRAS*, 273, L68
- Nordtvedt K., 1990, *Phys. Rev. Lett.*, 65, 953
- Phinney E.S., Kulkarni S.R., 1994, *Annu. Rev. Astron. Astrophys.*, 32, 591
- Phinney E.S., 1992, *Phil. Trans. R. Soc., Lond. A*, 341, 39
- Roy A. E., 1988, *Orbital Motion*, Institute of Physics Publishing, Bristol and Philadelphia
- Sandhu J.S., Bailes M., Manchester R.N., Navarro J., Kulkarni S.R., Anderson S.B., 1997, *ApJ*, 478, L95
- Sarna M.J., Antipova J., Muslimov A., 1998, *ApJ*, 499, 407
- Shklovskii I.S., 1970, *Sov. Astron.* 15, 562
- Standish E. M., 1990, *A&A*, 233, 252
- Taylor J.H., 1991, *Proc. IEEE*, 79, p. 1054-1062
- Taylor J.H. & Cordes J.M., 1993, *ApJ*, 411, 674
- Taylor J.H. & Weisberg J.M., 1989, *ApJ*, 345, 434
- Thorsett S.E., Arzoumanian Z., Camilo F., Lyne A.G., 1999, *ApJ*, 523, 763
- Toscano M., Sandhu J.S., Bailes M., Manchester R.N., Britton M.C., Kulkarni S.R., Anderson S.B., Stappers B.W., 1999a, *MNRAS*, 307, 925
- Toscano M., Britton M.C., Manchester R.N., Bailes M., Sandhu J.S., Kulkarni S.R., Anderson S.B., 1999b, *ApJ*, 523, L171
- van Kerkwijk M.H., Bergeron P. & Kulkarni S.R., 1996, *ApJ*, 467, L89
- Wex N., 2000, in *IAU Colloquium 177, Pulsar Astronomy – 2000 and Beyond*, eds. Kramer M., Wex N., Wielebinski R., ASP Conference Series, 202, 113
- Will C.M., Nordtvedt K., 1972, *ApJ*, 177, 757
- Will C.M., 1993, *Theory and Experiment in Gravitational Physics*, Cambridge University Press
- Williams J.G., Newhall X.X., Dickey J.O., 1996, *Phys. Rev. D*, 53, 6730

## APPENDIX A: TIMING OF SMALL-ECCENTRICITY BINARY PULSARS

Neglecting relativistic effects and parallax, the barycentric arrival time,  $t_b$ , of a signal emitted by a pulsar in an orbit around a compact companion is given by

$$t_b - t_0 = T + \Delta_R(T). \quad (\text{A1})$$

$T$  denotes the time of emission of the pulse signal as measured in the reference frame of the pulsar, i.e., it is directly related to the rotational phase  $\phi$  of the pulsar by

$$\phi \equiv \phi_0 + \nu T + \frac{1}{2} \dot{\nu} T^2 + \dots \quad (\text{A2})$$

The Roemer delay,  $\Delta_R$ , caused by the orbital motion of the pulsar is given by (Blandford & Teukolsky 1976)

$$\Delta_R = x \left[ (\cos U - e) \sin \omega + \sin U (1 - e^2)^{1/2} \cos \omega \right]. \quad (\text{A3})$$

where the eccentric anomaly,  $U$ , is determined by Kepler's equation

$$U - e \sin U = n_b (T - T_0), \quad n_b \equiv 2\pi/P_b, \quad (\text{A4})$$

and  $\omega$  denotes the longitude of periastron.

For small-eccentricity binary pulsars, however, the location of periastron is not a prominent feature in the TOAs. Therefore, modeling the timing data of small-eccentricity binary pulsars with equation (A3) leads to very high correlations between the parameters  $\omega$  and  $T_0$ . As a result,  $\omega$  and  $T_0$  show unacceptably large uncertainties in the  $\chi^2$  estimation of these parameters.

### A1 A timing model for small-eccentricity binary pulsars

Neglecting terms of order  $e^2$  the orbital motion  $\mathbf{X} = R(\cos \varphi, \sin \varphi, 0)$  of a pulsar in a small-eccentricity binary system, is given by (see, e.g., Roy 1988)

$$\left. \begin{aligned} R &= a_p (1 - e \cos M) \\ \varphi &= M + 2e \sin M \end{aligned} \right\} M = n_b (T - T_0), \quad (\text{A5})$$

where  $M = \varphi = 0$  corresponds to the location of periastron. To first order approximation in the small eccentricity  $e$  the Roemer delay (Eq. A3) can therefore be written as

$$\Delta_R \simeq x \left( \sin \Phi + \frac{\kappa}{2} \sin 2\Phi - \frac{\eta}{2} \cos 2\Phi \right), \quad (\text{A6})$$

$$\Phi = n_b (T - T_{\text{asc}}),$$

where terms which are constant in time are omitted. The three Keplerian parameters  $T_0$ ,  $e$ , and  $\omega$  are replaced by the *time of ascending node* which is defined by

$$T_{\text{asc}} \equiv T_0 - \omega/n_b, \quad (\text{A7})$$

and the *first and second Laplace-Lagrange parameter*,

$$\eta \equiv e \sin \omega \quad \text{and} \quad \kappa \equiv e \cos \omega, \quad (\text{A8})$$

respectively. Note that the actual time when the pulsar passes through the ascending node is given by  $T_{\text{asc}} + 2\eta/n_b$ . The time of conjunction is given by  $T_{\text{asc}} + P_b/4 - 2\kappa/n_b$ .

Eq. (A6) accounts only for first-order corrections in  $e$ . Therefore, the difference between the exact expression (A3) and Eq. (A6) can grow up to  $xe^2$ . For most of the low eccentricity binary pulsars, the error in the TOA measurements

is much larger than  $xe^2$  and thus the linear-in- $e$  model is sufficient.

Secular changes in the parameters  $n_b$ ,  $x$ ,  $e$ , and  $\omega$  in Eq. (A3) are accounted for in the new timing model by using

$$\Phi = \bar{n}_b (T - T_{\text{asc}}) + \frac{1}{2} \dot{\bar{n}}_b (T - T_{\text{asc}}), \quad (\text{A9})$$

and

$$\begin{aligned} x &= x_0 + \dot{x} (T - T_{\text{asc}}), \\ \eta &= \eta_0 + \dot{\eta} (T - T_{\text{asc}}), \\ \kappa &= \kappa_0 + \dot{\kappa} (T - T_{\text{asc}}), \end{aligned} \quad (\text{A10})$$

in Eq. (A6) where the relations

$$\bar{n}_b = n_b + \dot{\omega} - \dot{n}_b (T_0 - T_{\text{asc}}), \quad (\text{A11})$$

$$T_{\text{asc}} = T_0 - \frac{\omega_0}{n_b + \dot{\omega}}, \quad (\text{A12})$$

$$\dot{\bar{n}}_b = \dot{n}_b, \quad (\text{A13})$$

$$\dot{\eta} = \dot{e} \sin \omega + e \cos \omega \dot{\omega}, \quad (\text{A14})$$

$$\dot{\kappa} = \dot{e} \cos \omega - e \sin \omega \dot{\omega} \quad (\text{A15})$$

hold.

### A2 Small-eccentricity orbits and Shapiro delay

For small-eccentricity binary pulsars, the Shapiro delay can be written as

$$\Delta_S = -2r \ln(1 - s \sin \Phi), \quad (\text{A16})$$

where  $r = Gm_c/c^3$  and  $s = \sin i$ . As a Fourier series Eq. (A16) takes the form

$$\Delta_S = 2r(a_0 + b_1 \sin \Phi - a_2 \cos 2\Phi + \dots), \quad (\text{A17})$$

where

$$a_0 = -\ln \left( \frac{1 + \sqrt{1 - s^2}}{2} \right), \quad (\text{A18})$$

$$b_1 = 2 \frac{1 - \sqrt{1 - s^2}}{s}, \quad (\text{A19})$$

$$a_2 = 2 \frac{1 - \sqrt{1 - s^2}}{s^2} - 1. \quad (\text{A20})$$

Only for orbits where  $\sqrt{1 - s^2} \ll 1$  (nearly edge-on) are higher harmonics, indicated as ... in Eq. (A17), significant. Otherwise, the Shapiro delay cannot be separated from the Roemer delay. Consequently the observed values for  $x$  and  $\eta$  differ from their intrinsic values by

$$x^{(obs)} = x + 2rb_1, \quad (\text{A21})$$

$$\eta^{(obs)} = \eta + 4ra_2/x, \quad (\text{A22})$$

as can be seen by a comparison of Eq. (A17) with Eq. (A6). In terms of the Blandford-Teukolsky model, Eq. (A22) means that the observed value of the eccentricity  $e$  and the observed value of the longitude of periastron  $\omega$  are different from the intrinsic values of these parameters.

This new model has been implemented in the TEMPO timing software as binary model ELL1.